Dynamic Slip Transfer from the Denali to Totschunda Faults, Alaska

Testing Theory for Fault Branching

Harsha S. Bhat [1], Renata Dmowska [1,2], James R. Rice [1,2] and Nobuki Kame [3]

(1) Division of Engineering and Applied Sciences, Harvard University

(2) Department of Earth and Planetary Sciences, Harvard University

(3) Department of Earth and Planetary Sciences, Faculty of Science, Kyushu University

Abstract

We analyze dynamic slip transfer from the Denali to Totschunda faults during the M_w 7.9, November 3, 2002, Denali, Alaska, earthquake. This adopts the theory and methodology of *Poliakov et al. [2002]* and *Kame et al. [2003]*, in which it was shown that the propensity of the rupture path to follow a fault branch is determined by the preexisting stress state, branch angle and incoming rupture velocity at the branch location. Here we check that theory on the Denali-Totschunda rupture process using 2D numerical simulations of processes in the vicinity of the branch junction.

We simulate slip transfer by a 2D elastodynamic boundary integral equation model of mode II slip-weakening rupture with self-chosen path along the branched fault system. All our simulations except for 70^o and $0.9c_s$ predict that the rupture path branches off along Totschunda without continuation along Denali. In that exceptional case there is also continuation of rupture along Denali at a speed slower than that along Totschunda and with smaller slip.

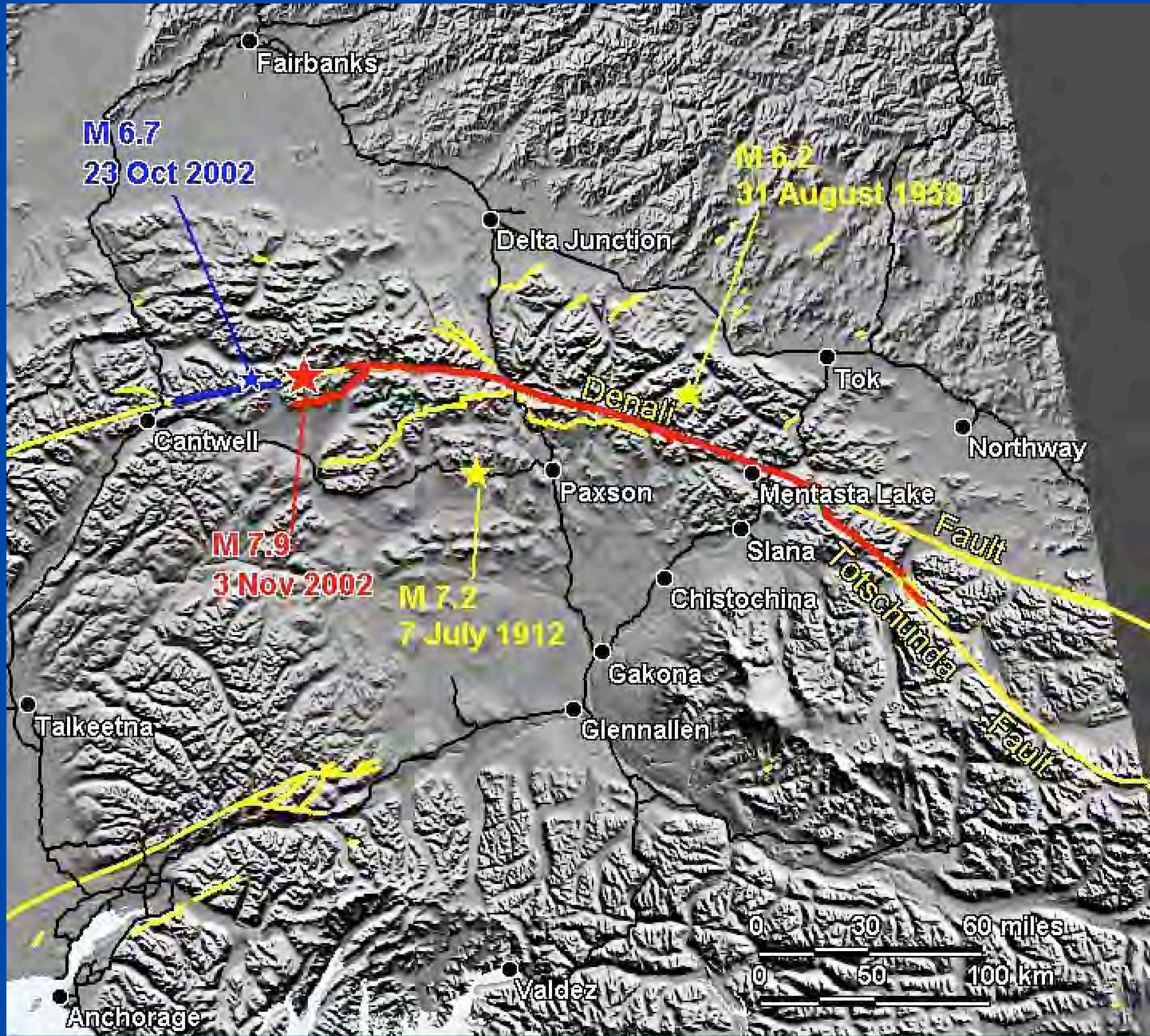

Figure 1. Rupture path, solid line, of the Mw 7.9 Denali earthquake. A star to towards the left of center of the figure marks the epicenter of the 3 November 2002 event [Figure courtesy: Alaska Division of Geological and Geophysical Surveys].

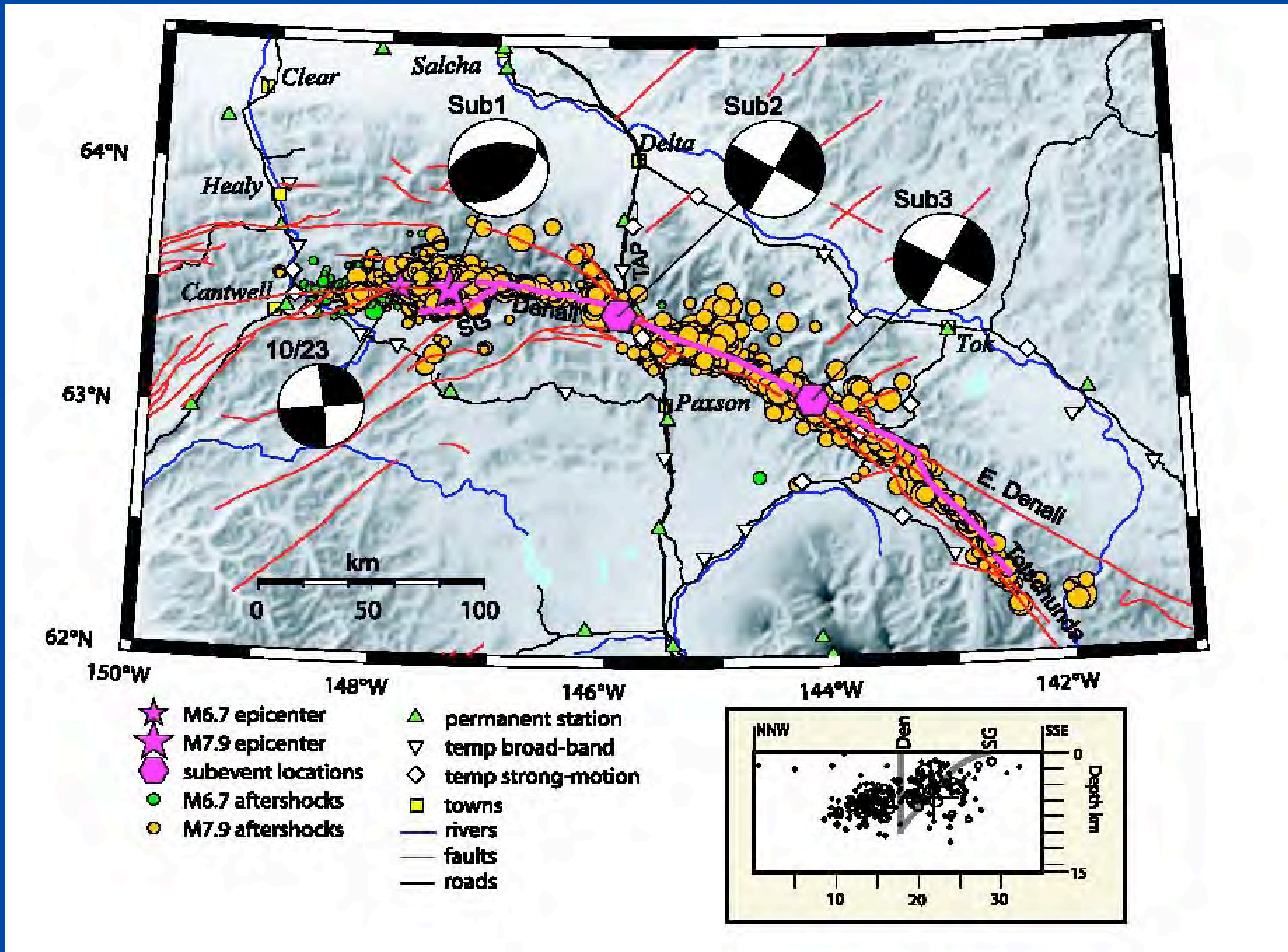

Figure 2. Aftershocks of the M_w 7.9 event, from Eberhart-Phillips *et al.* [2003], also showing three sub events during the rupture.

Three key parameters influence branching

(1) The pre-stress state. More specifically the orientation of the principal maximum stress with the main fault, *Ψ*.

(2) Rupture velocity near the branching region, v_r.

(3) Orientation of branch with respect to the main fault, φ.

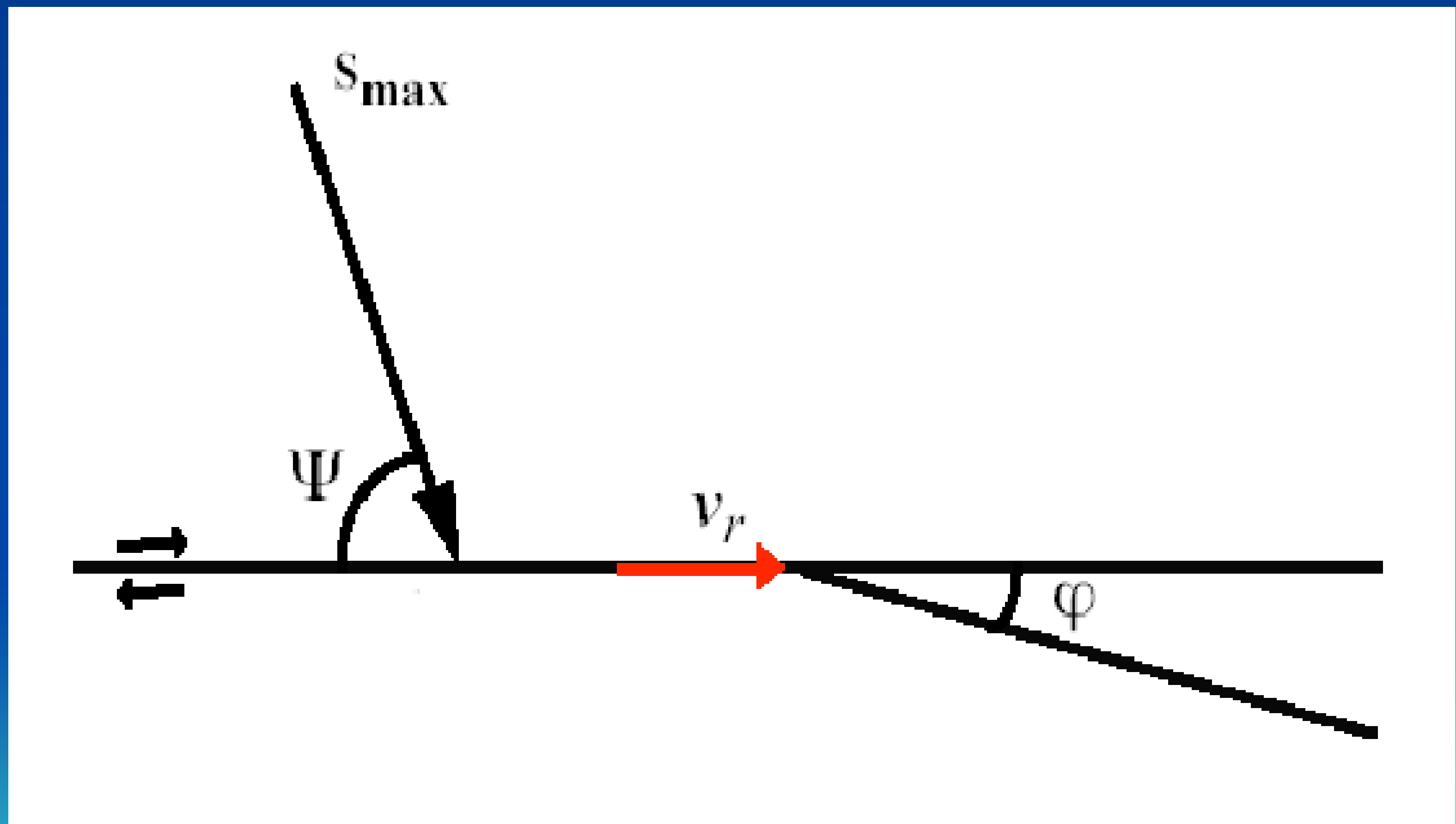

Figure 3. Fault geometry used in the model along with the associated parameters.

Failure Criterion (Boundary Condition)

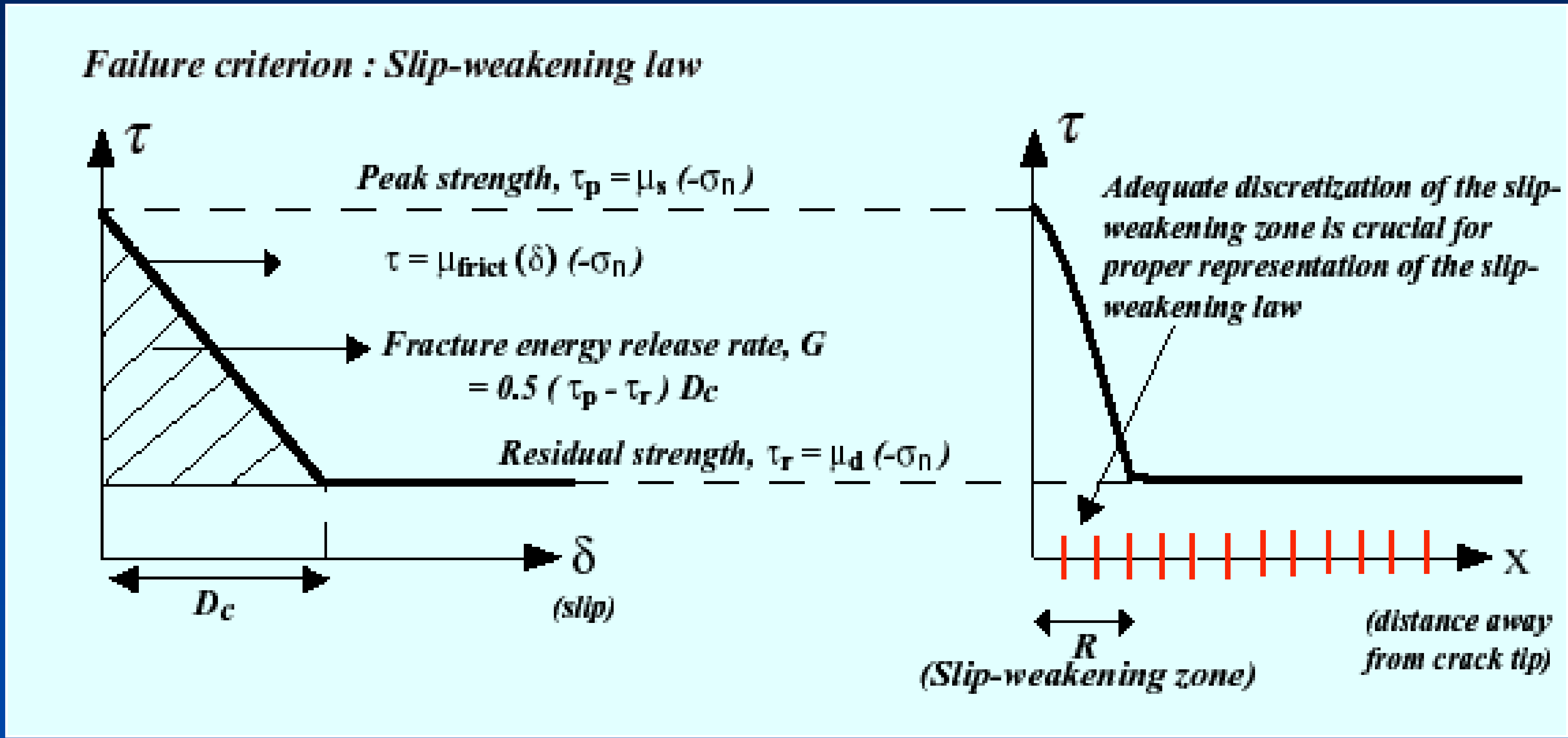

• **Complete 2D elastodynamic analysis of the branching phenomenon** using numerical methodology, the Boundary Integral Equation Method, based on Kame *et. al.* [2003].

• **Aim of current study not to simulate the entire event but just the branching phenomenon.**

The influence of branching angle (φ)

Figure 3.
Results of 2D numerical simulations from Kame *et al.* [2003] showing the influence of branching angle (φ) on a right-laterally propagating rupture at a velocity (v_r) of *$0.8c_s$* near branching location. The orientation angle *Ψ* of the principal maximum stress with respect to the main fault is *56^o*.

The solid black line shows the path of the rupture; unruptured fault regions shown in gray. c_s is the shear wave speed of the medium.

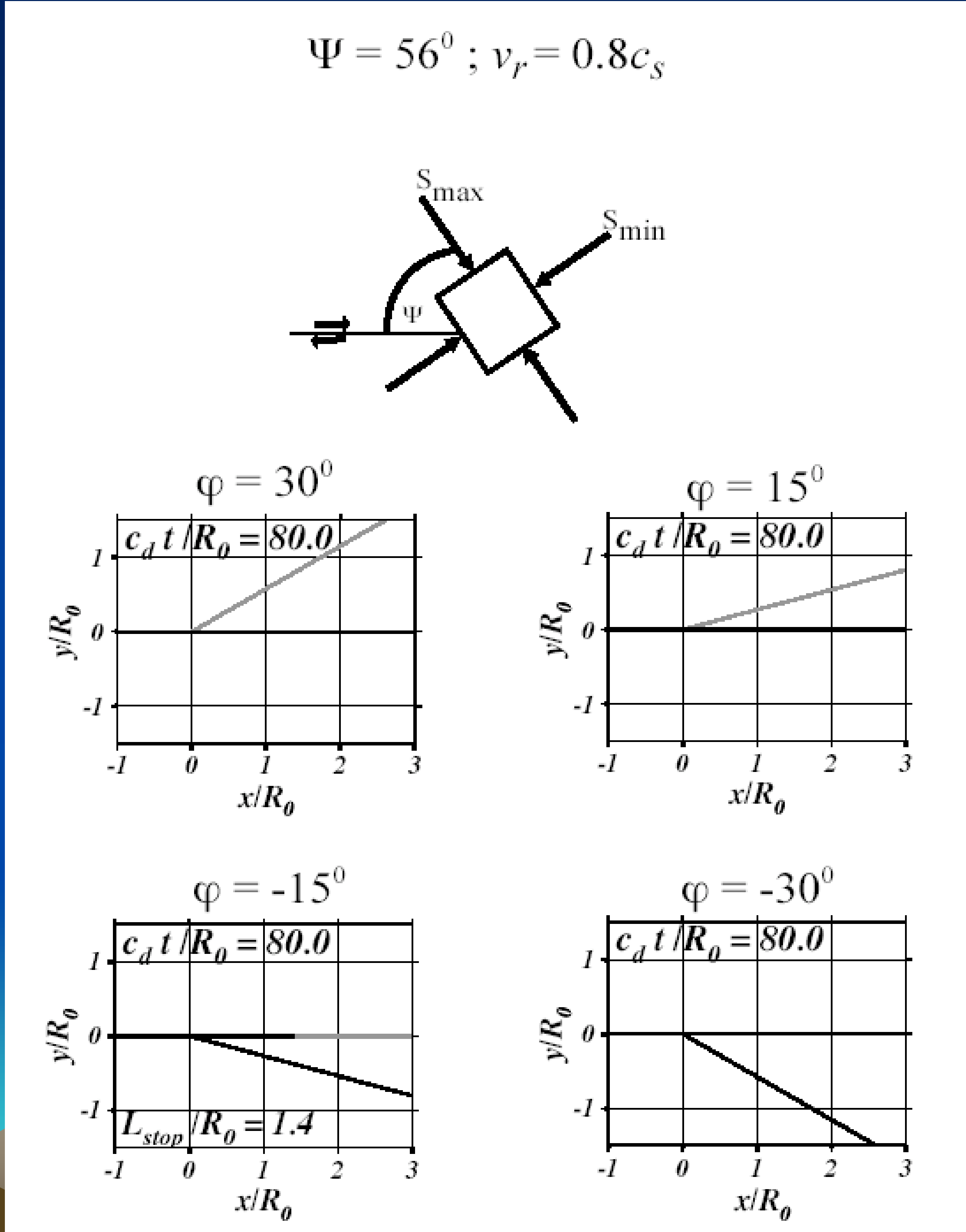

The influence of orientation of the principal maximum stress

Figure 4.
Results of 2D numerical simulations from Kame *et al.* [2003] showing the influence of orientation of the principal maximum stress with respect to the main fault (Ψ) on a right-laterally propagating rupture at a velocity (v_r) of $0.8c_s$ near branching location. The fault geometry is fixed with the branching angle $\varphi = -15^o$. with respect to the main fault of the principal maximum stress.

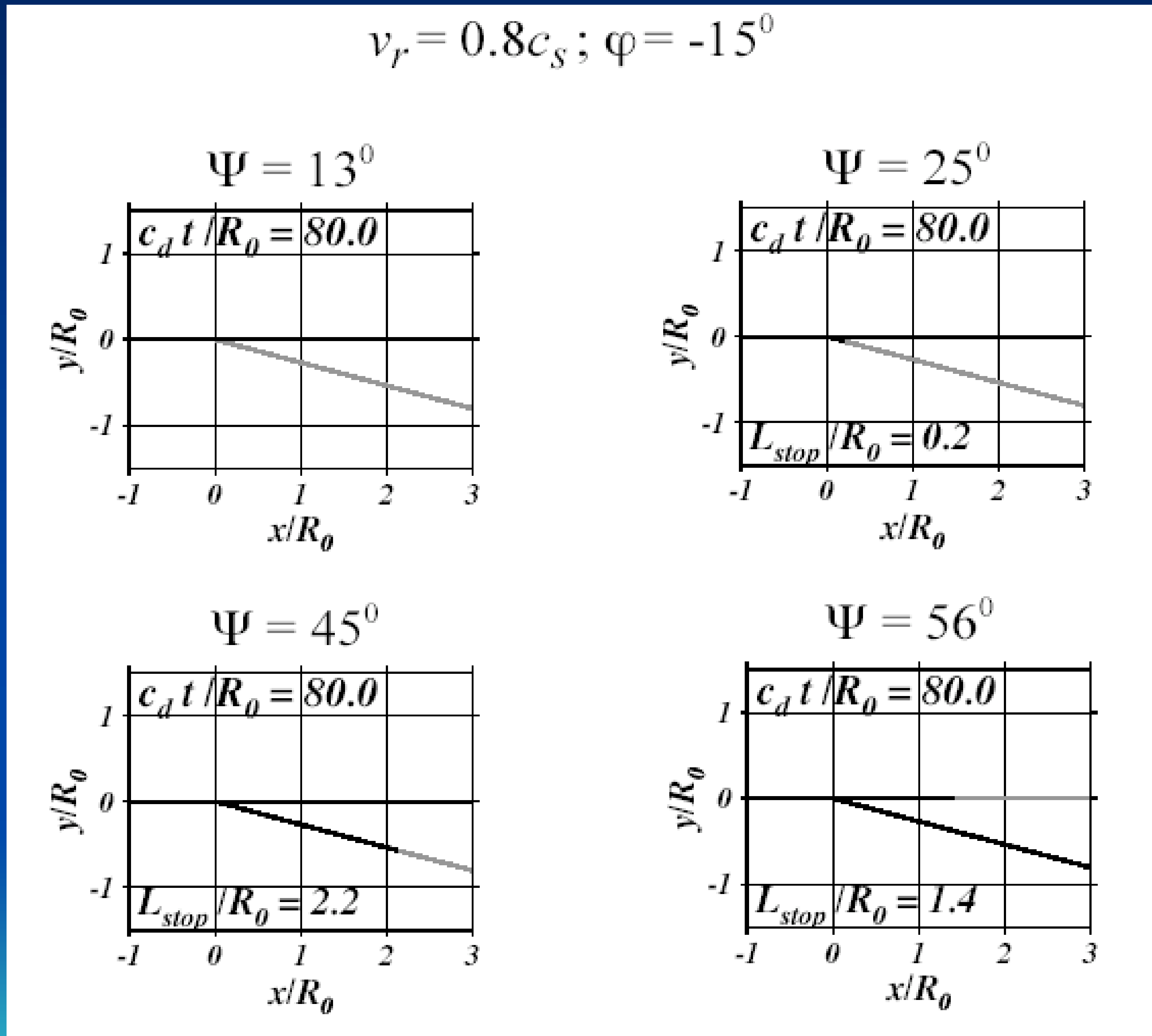

The influence of rupture velocity

Figure 5.
Results of 2D numerical simulations from Kame *et al.* [2003] showing the influence of rupture velocity at branching location (v_r) on a right-laterally propagating rupture approaching a branched fault segment at $\varphi = -15^o$. The orientation of the principal maximum stress with respect to the main fault (Ψ) is 56^o.

The solid black line shows the path of the rupture. c_s is the shear wave speed of the medium.

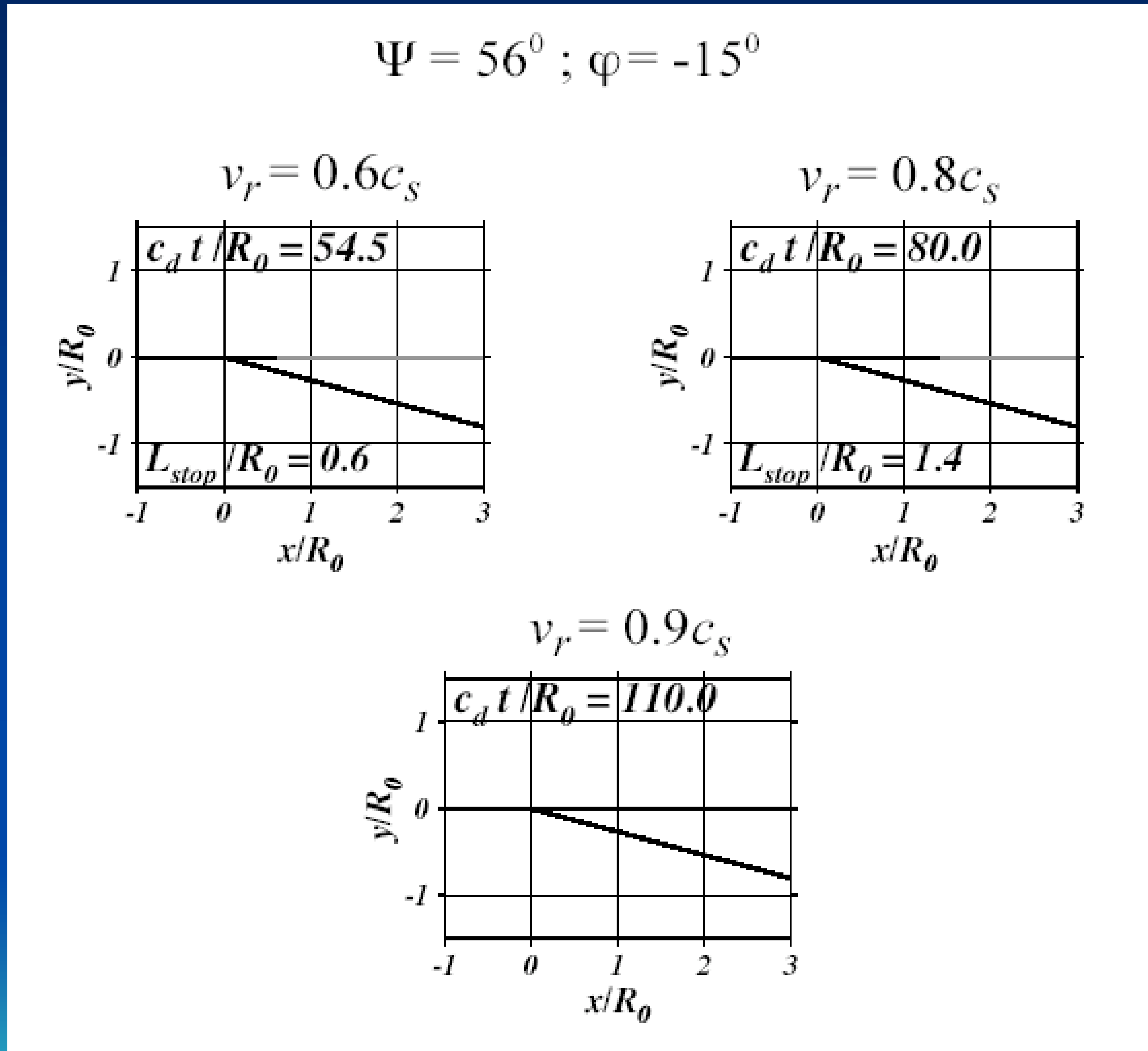

Branching parameters for Denali

- **Orientation of the principal maximum stress with the main fault, Ψ**

- **Inversion from focal mechanisms, volcanic, geologic fault and bore-hole breakout data**

  Nakamura et. al. [1980] and Estabrook et. al. [1988] : $\Psi \approx 75^0$

- **Inversion from focal mechanisms**

  Ratchkovski and Hansen [2002]: $\Psi \approx 73^0$

  Ratchkovski [2003]: $\Psi \approx 80^0$

- **Branching angle, φ**

  - **Savage and Lisowski [1991]: $\varphi \approx -15^0$ to the extensional side;**

- **Rupture velocity near the branching region, v_r: not well constrained**

  - **Kikuchi and Yamanaka [2002]: Average $v_r = 0.8c_s$**
  - **Ellsworth et. al. [2004]: $v_r > c_s$ near PS10. $v_r = 0.8c_s$ beyond PS10**

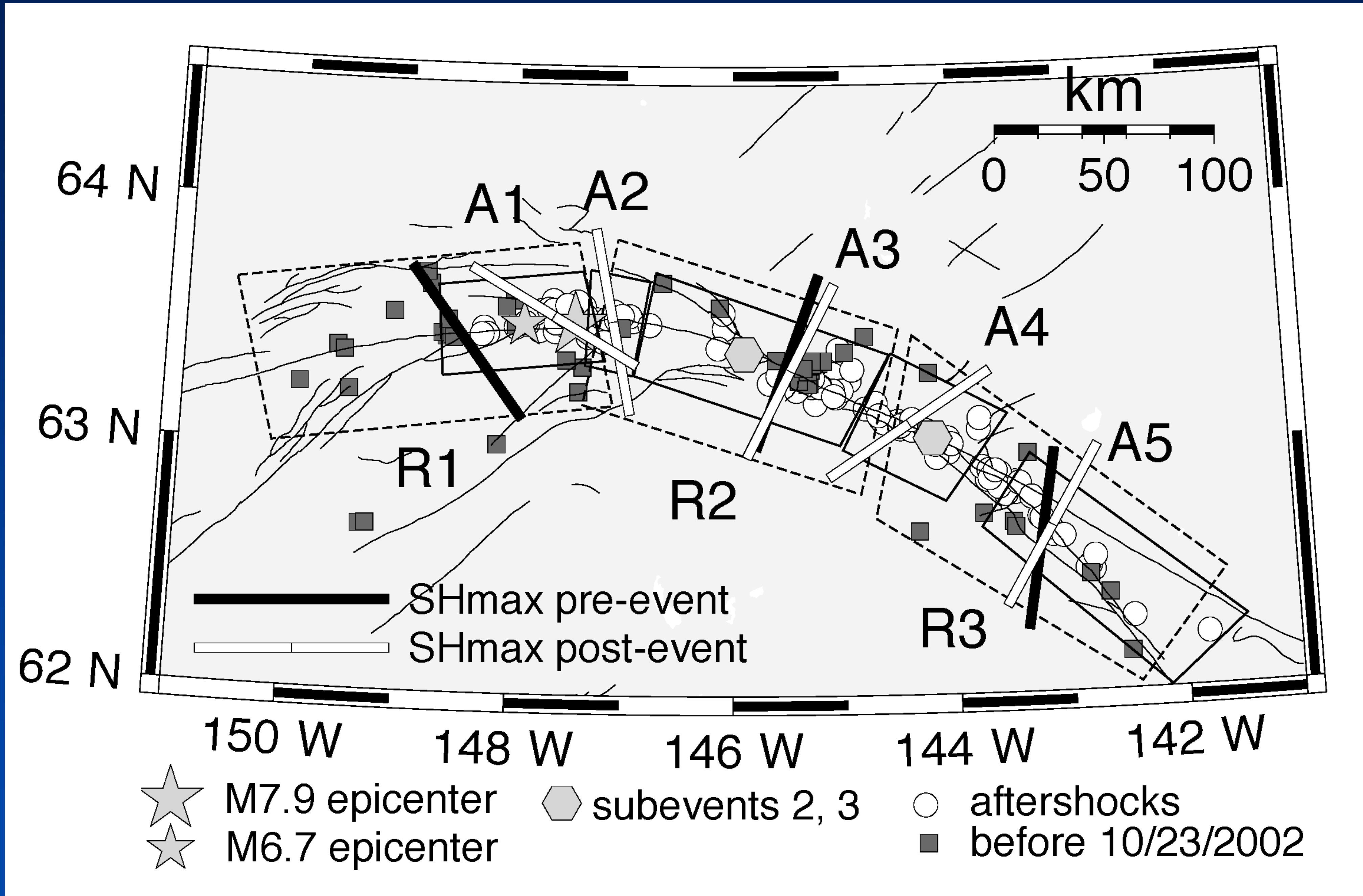

Figure 6. Maximum principal stress orientations prior to the 2002 Denali earthquake sequence (black bars) and for the 2002 Denali earthquake sequence aftershocks (white bars), from Ratchkovski [2003]. Dashed polygons outline inversion blocks for events prior to October 2002. Solid polygons are the inversion regions using the aftershocks. Solid lines are the mapped fault traces. Subevent locations [Eberhart-Phillips *et al.*, 2003] of the magnitude 7.9 earthquake are shown as hexagons.

Result of Case 1: **Only Totschunda fault self-chosen**

Figure 7.
Plot of slip velocity along the Denali and Totschunda fault segments for $Y=70^o$; $v_r=0.6c_s$ case. Slip velocity variation along Totschunda fault begins at $5X/R_0=58$.

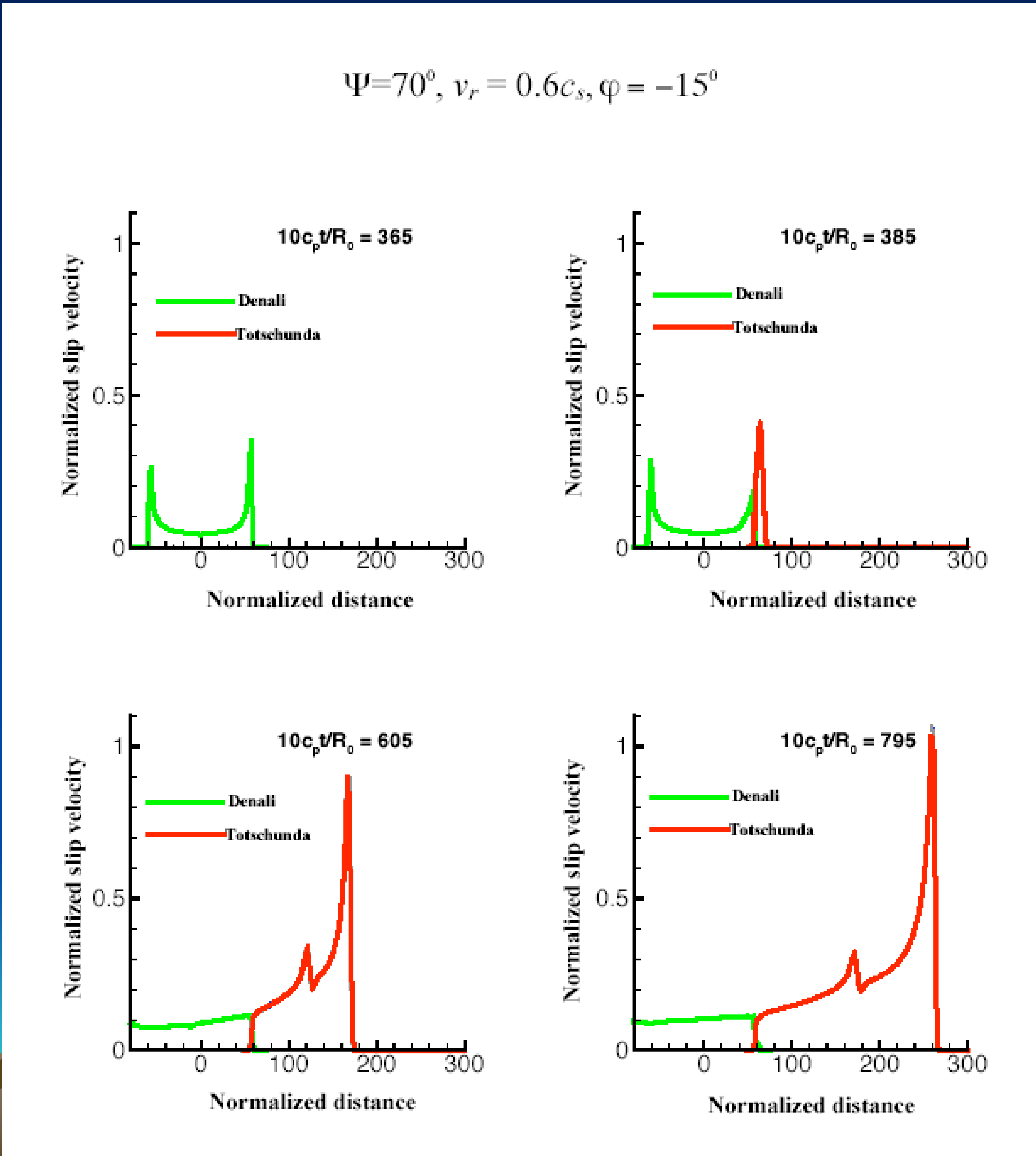

v_r : velocity near the branching point
c_s : S-wave speed of the medium
R_0 : size of the slip-weakening zone
μ : shear modulus of the medium
v : slip velocity,
$-\sigma^0_{yy}$: initial normal compressive stress
c_p : P-wave velocity of the medium

Result of Case 2: Only Totschunda fault self-chosen

Figure 8.
Plot of slip velocity along the Denali and Totschunda fault segments for $\Psi = 70^o$; $v_r = 0.8c_s$ case. Slip velocity variation along Totschunda is projected on the Denali fault. Totschunda fault begins at $5X/R_0 = 108$

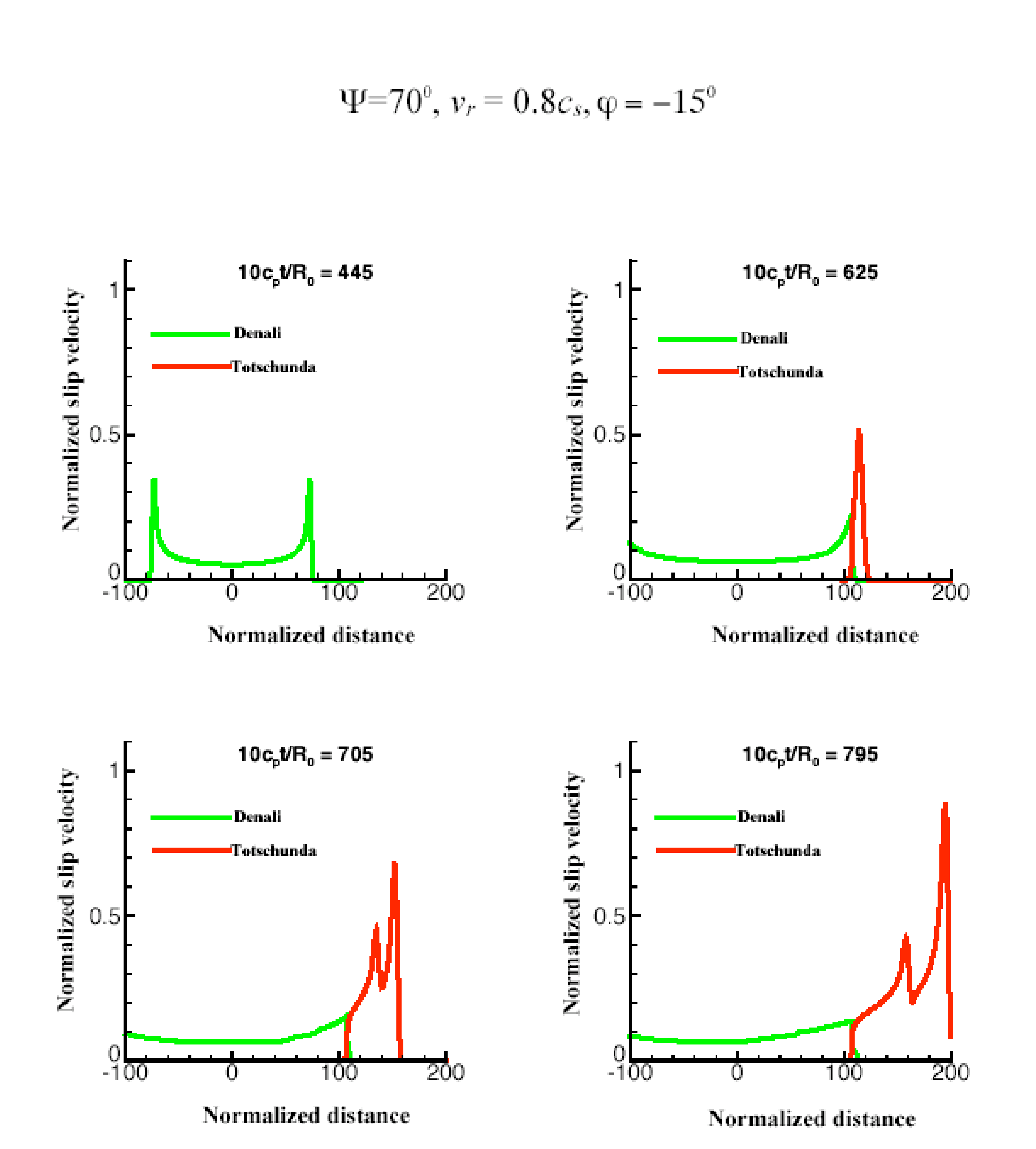

Result of Case 3: Both Totschunda and Denali faults self-chosen

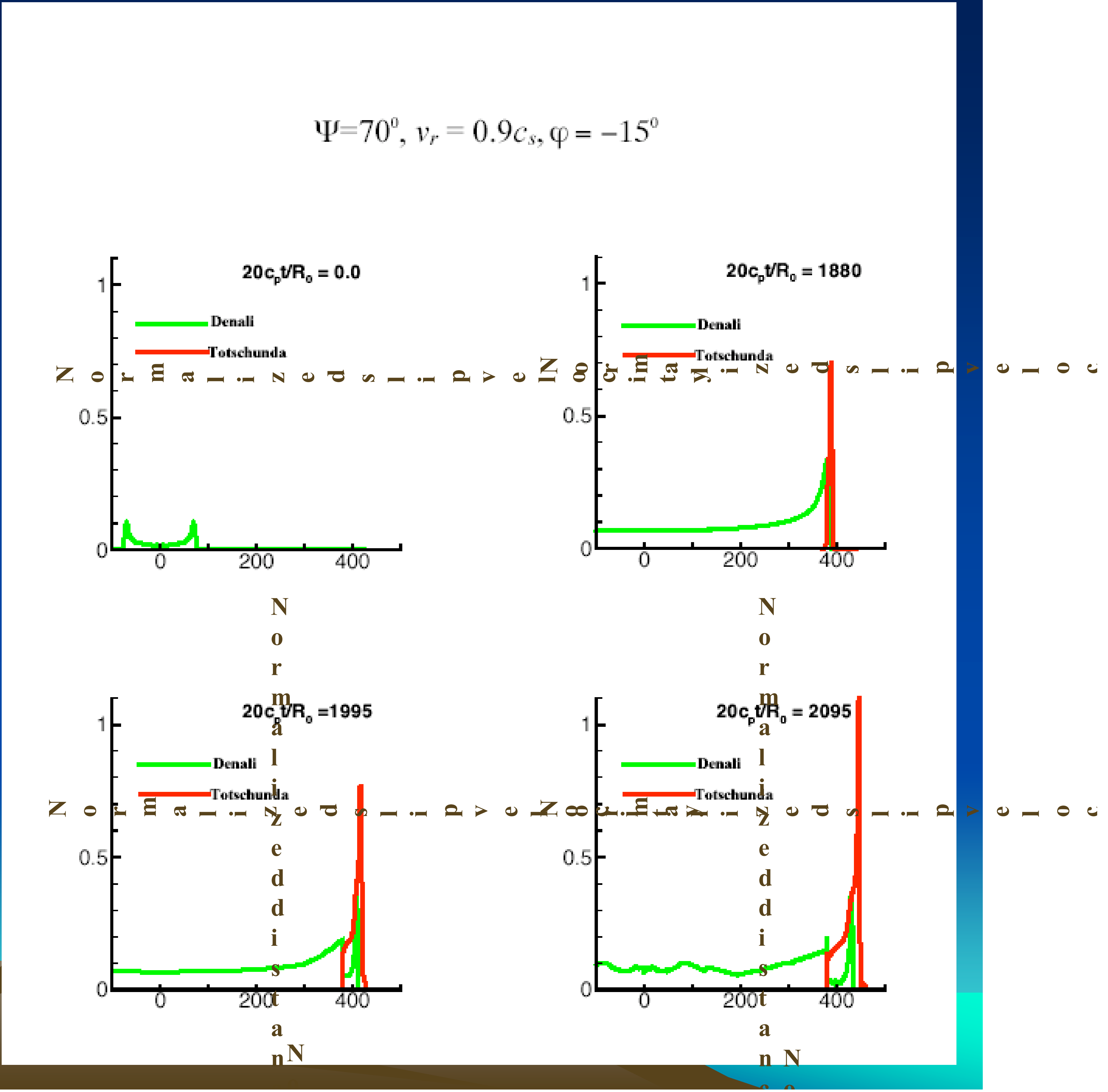

Figure 9.
Plot of slip velocity along the Denali and Totschunda fault segments for *Ψ = 70°*; *v_r = 0.9c_s* case. Slip velocity variation along Totschunda is projected on the Denali fault. Totschunda fault begins at *10X/R_0 = 380*.

Result of Case 4: Only Totschunda fault self-chosen

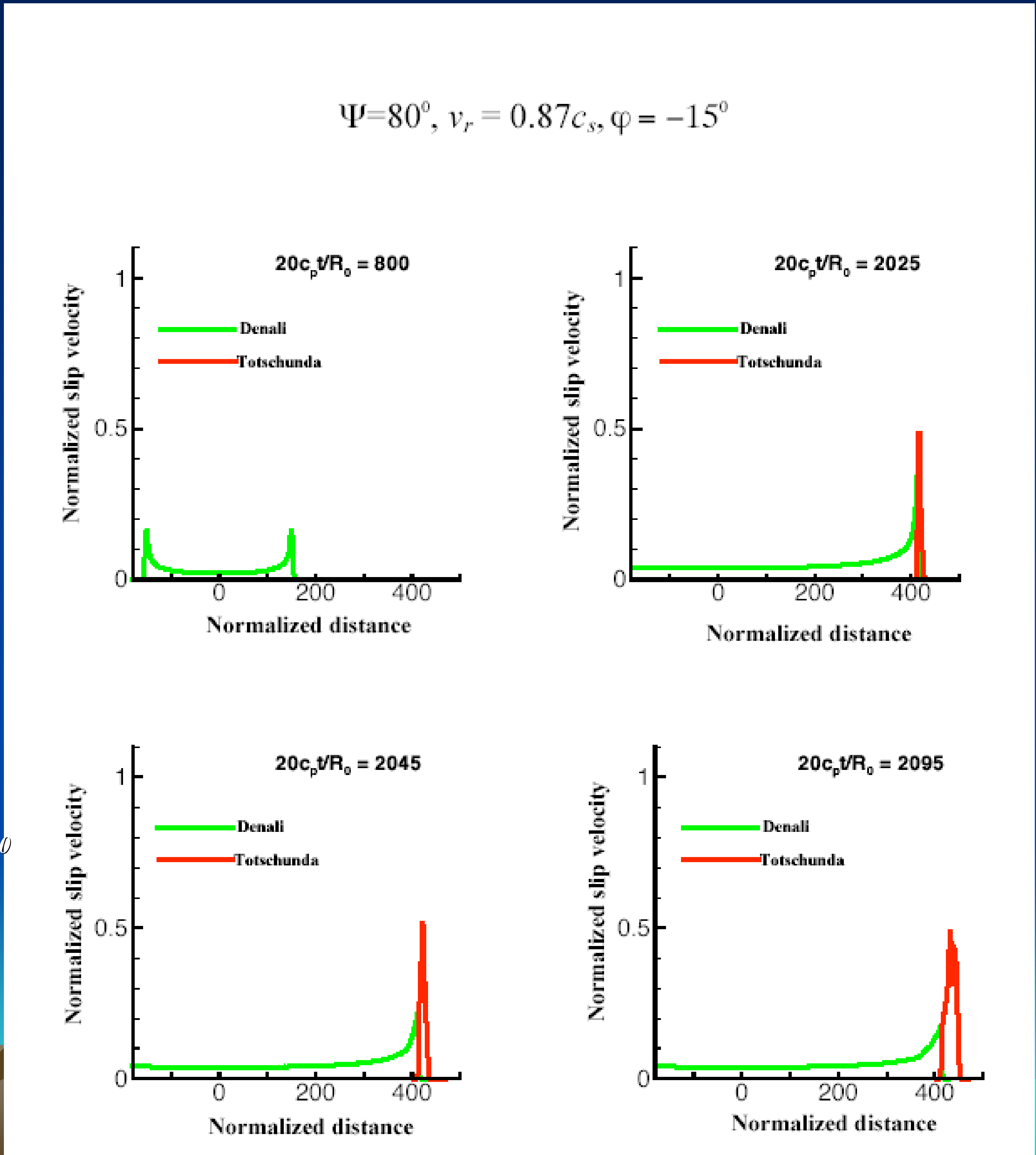

Figure 10.
Plot of slip velocity along the Denali and Totschunda fault segments for *$\Psi = 80^o$*; *$v_r = 0.87c_s$* case. Slip velocity variation along Totschunda is projected on the Denali fault. Totschunda fault begins at *$10X/R_0 = 414$*.

Result of Case 5: Only Totschunda fault self-chosen

Figure 11.
Plot of slip velocity along the Denali and Totschunda fault segments for *$\Psi = 70^o$*; *$v_r = 1.4c_s$*. Slip velocity variation along Totschunda is projected on the Denali fault. Totschunda fault begins at *$10X/R_0 = 104$*.

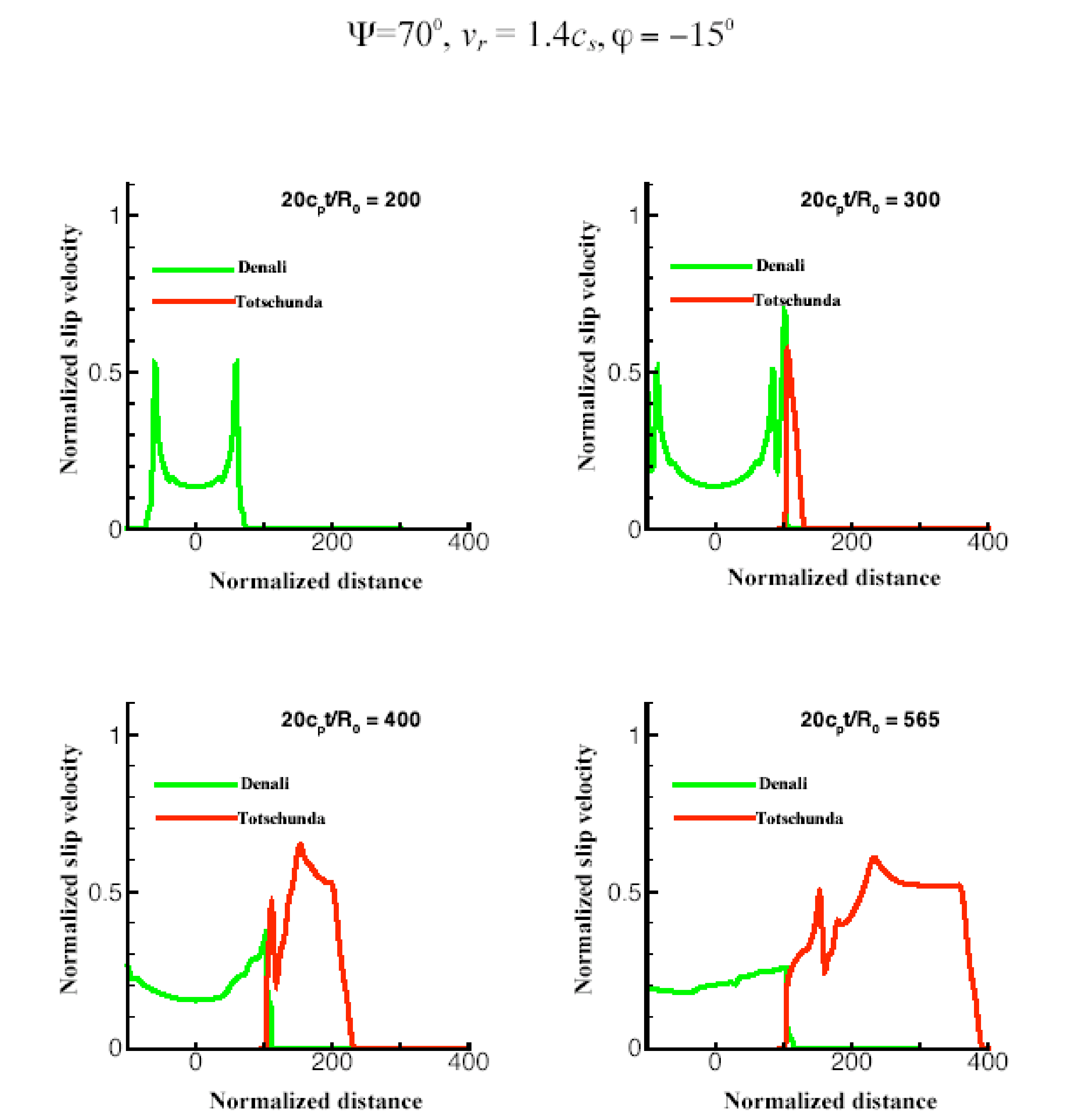

Variation of rupture velocity

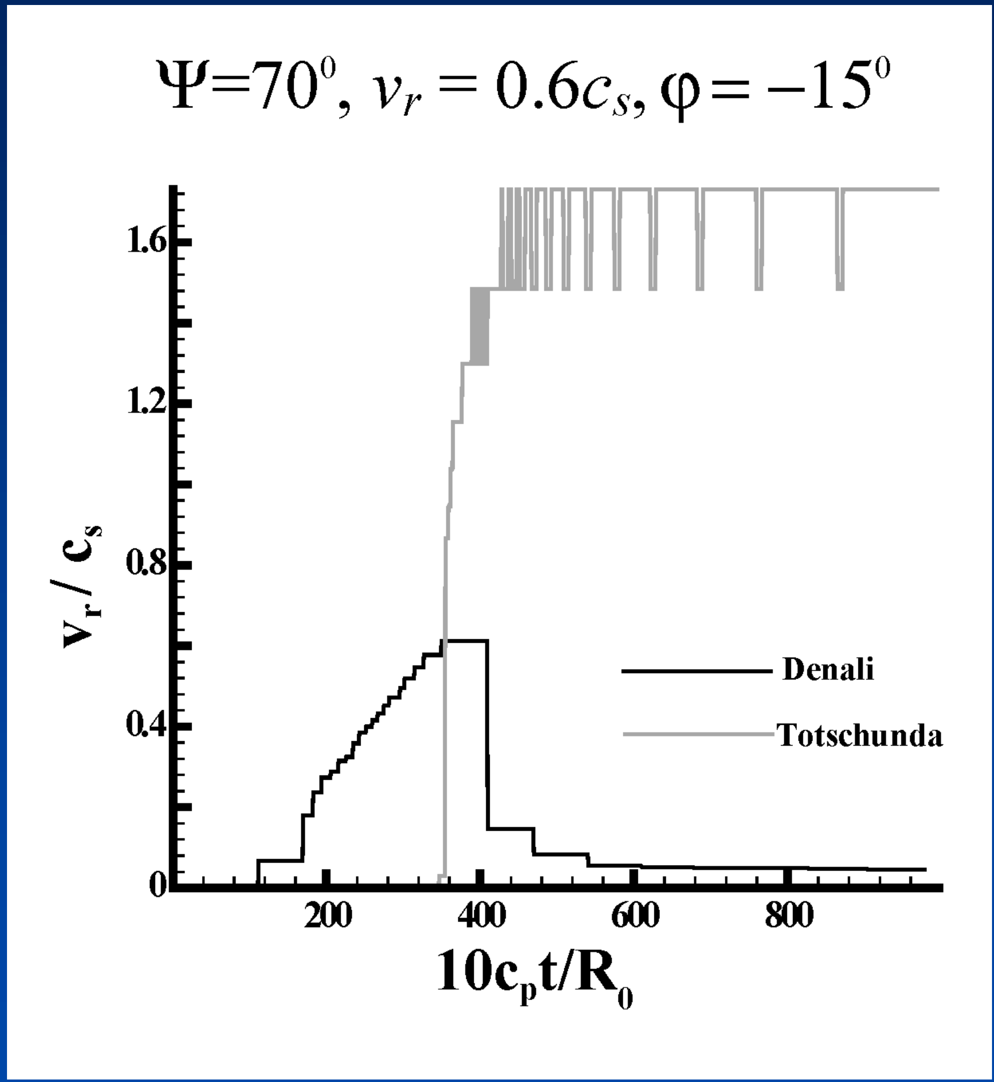

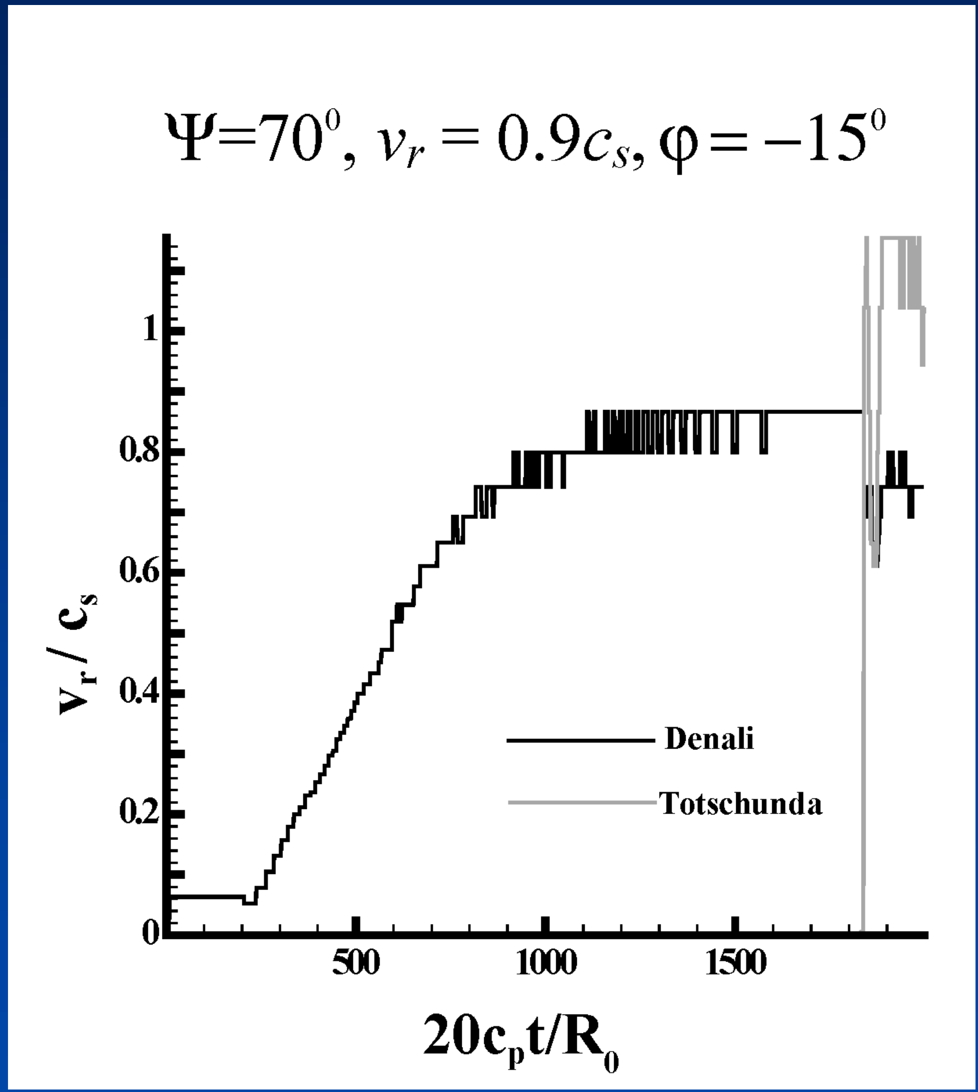

Figure 12.
Variation of rupture velocity along the Denali and the Totschunda fault segments for $\Psi = 70^o$; $v_r = 0.6c_s$ and $\Psi = 70^o$; $v_r = 0.9c_s$ cases. Rupture velocity is determined as the time taken to advance three spatial cells and thus the possible values of rupture velocity are quantized.

Summary and Conclusions

- **2D elastodynamic analysis of the branching phenomenon using theoretical and numerical methodologies outlined by *Poliakov et al. [2002]* and *Kame et al. [2003]*.**

- **Strength of the fault assumed to follow slip-weakening behavior.**

- **Performed numerical investigations for various parameters that influence branching as outlined by *Kame et al. [2003]*.**

- **Except for the case when $\Psi = 70^0$ and $v_r = 0.9c_s$ all simulations show that the rupture continues exclusively on the Totschunda fault beyond the branching point, in agreement with observations.**